1. Bricknell, I. and Dalmo, R. A., The use of immunostimulants in fish larval aquaculture. *Fish Shellfish Immunol*., 2005, **19**, 457–472.
2. Montero-Rocha, A., McIntosh, D., Sanchez-Merino, R. and Flores, I., Immunostimulation of white shrimp (*Litopenaeus vannamei*) following dietary administration of Ergosan. *J. Invertebr. Pathol*., 2006, **91**(3), 188–194.
3. Yusoff, F. M., Shariff, M., Lee, Y. K. and Banerjee, S., Preliminary study on the use of *Bacillus* sp., *Vibrio* sp. and egg white to enhance growth, survival rate and resistance of *Penaeus monodon* (Fabricius) to white spot syndrome virus. *Asian Australas. J. Anim. Sci*., 2001, **14**, 1477–1480.
4. Karen Grace, S. A., Mary Jane, S. A., Rosy, L. J. and Valeriano Jr, L. C., Effects of dietary mannan oligosaccharide (MOS) and β-glucan on growth, immune response and survival against white spot syndrome virus (WSSV) infection of juvenile tiger shrimp *Penaeus monodon*. *AACL Bioflux*, 2014, **7**(5), 321–332.
5. Raa, J., The use of stimulants in fish and shellfish feeds. University of Troms, Norway, 2000, pp. 240–251.
6. Sakai, M., Current research status of fish immunostimulants. *Aquaculture*, 1998, **172**, 63–92.
7. Akbari, M., Heidarieh, M., Mirvaghefi, A., Farahmand, H., Sheikhzadeh, N. and Najafi Hajivar, E., Effect of dietary Ergosan and Hilyses on growth performance, hematological variables and immune response in rainbow trout (*Oncorhynchus mykiss*). *Iran. J. Aquat. Anim. Heal*., 2014, **1**(1), 1–6.
8. SPAHAC, Brief about Aquavac Ergosan and Aquavac Vibromax vaccine. Schering-Plough Animal Health Aquaculture Corporation, New Jersey, USA, 2005; www.spaquaculture.com
9. Brugger, S. D., Baumberger, C., Jost, M., Jenni, W., Brugger, U. and Muhlemann, K., Automated counting of bacterial colony forming units on agar plates. *PLoS ONE*, 2012, **7**(3), 3–7.
10. Excel, Microsoft Office Professional. Microsoft, USA, 2007.
11. Heidarieh, M., Afsharnasa, M., Soltani, M., Dashtyanna, A., Rajabifar, S., Sheikhzade, N. and Tamimi, A. H., Effects of Ergosan and Vibromax to prevent vibriosis and WSSV in *Litopeaneus vannamei*. *J. Fish. Aquat. Sci*., 2010, **5**(2), 120–125.
12. Valeriano, L. C., Vianney, T. O., Rex Ferdinand, M. T., Nieves, A. T., Gaudiosa, S. G., Leobert, D. P. and Karen Grace, S. A., Ergosan as immunostimulant: effects of dose and frequency on growth performance, immune responses and white spot syndrome virus resistance in tiger shrimp, *Penaeus monodon*. In Asian-Pacific Aquaculture Meeting Abstract, Iloilo, Philippines, 2013.
13. Bahri, A. H., Azari Takami, G. H. and Mohammadizadeh, F., The study of alginic acid (Ergosan) on growth and survival rates in Indian white shrimp post larvae (*Fenneropenaeus indicus*). *J. Aquat. Anim. Fish*., 2010, **1**(3), 1–10.
14. Heidarieh, M., Mirvaghefi, A. R., Akbari, M., Farahmand, H., Sheikhzadeh, N., Shahbazfar, A. A. and Behgar, M., Effect of dietary Ergosan on growth performance, digestive enzymes, intestinal histology, hematological parameters and body composition of rainbow trout (*Oncorhynchus mykiss*). *Fish Physiol. Biochem*., 2012, **38**(4), 1169–1174.
15. Jalali, M. A., Ahmadifar, E., Sudagar, M. and Takami, G. A., Growth efficiency, body composition, survival and hematological changes in great sturgeon (*Huso huso* Linnaeus, 1758) juveniles fed diets supplemented with different levels of Ergosan. *Aquacult. Res*., 2009, **40**, 804–809.
16. Peddie, S., Zou, J. and Secombes, C. J., Immunostimulation in the rainbow trout (*Oncorhynchus mykiss*) following intraperitoneal administration of Ergosan. *Vet. Immunol. Immunopathol*., 2002, **86**, 101–113.
17. Gioacchini, G., Lombardo, F., Avella, M. A., Olivotto, I. and Carnevali, O., Welfare improvement using alginic acid in rainbow trout (*Oncorhynchus mykiss*) juveniles. *Chem. Ecol*., 2010, **26**, 111–121.
18. Heidarieh, M., Soltani, M., Tamimi, A. H. and Toluei, M. H., Comparative effect of raw fiber (Vitacel) and alginic acid (Ergosan) on growth performance, immunocompetent cell population and plasma lysozyme content of giant sturgeon (*Huso huso*). *Turk. J. Fish. Aquat. Sci*., 2011, **11**, 445–450.

ACKNOWLEDGEMENT. We thank the Director, National Aquaculture Group, Saudi Arabia for providing the necessary facilities.

Received 2 May 2016; revised accepted 3 June 2016

doi: 10.18520/cs/v114/i08/1760-1762

Spectral modelling of estuarine coloured dissolved organic matter

Nittala S. Sarma[1,*], Sudarsana Rao Pandi[1], N. V. H. K. Chari[1], Gundala Chiranjeevulu[1], Rayaprolu Kiran[1], K. Shiva Krishna[1], D. Bhaskara Rao[1], P. Venkatesh[1], B. Charan Kumar[2] and A. V. Raman[2]

[1]Marine Chemistry Laboratory,
[2]Marine Biological Laboratory, Andhra University,
Visakhapatnam 530 003, India

Measuring coloured dissolved organic matter (CDOM) holds advantage over dissolved organic carbon (DOC) determination, as it can be remotely estimated unlike the latter, for which it can potentially act as a proxy. The CDOM absorbance, by definition, falls exponentially with wavelength of light (λ) in the ultraviolet-visible region. Investigating over 800 absorption spectra of water samples from the tropical monsoonal Godavari estuary and the Chilika brackish water lagoon, we found that the spectral slope (S) of the 330–440 nm region ($S_{330–440}$) is best suited to retrieve CDOM and its exponential character.

Keywords: CDOM, Chilika lagoon, Godavari estuary, spectral slope, $S_{330–440}$, UV-visible absorbance.

COLOURED (or chromophoric) dissolved organic matter (CDOM) is the optically active fraction of DOM[1]. The CDOM measurement is credited as an alternative means of quantifying dissolved organic carbon, although the conversion equations are region-specific[2–7]. The ease of CDOM measurement in terms of absorption coefficient (or absorbance) in the UV-visible region of electromagnetic radiation provides an advantage in the study of the cycling of DOM. The source, structure and interactions in

*For correspondence. (e-mail: nssarma@rediffmail.com)

the environment of CDOM[1,5] as well as its role in chlorophyll retrieval by remote sensing satellites[8] have been subjects of extensive studies.

CDOM has been found to obey the inverse exponential law, $A(\lambda) = k \cdot \exp(-s\lambda)$, according to which the absorbance $A(\lambda)$ falls exponentially on proceeding from shorter towards longer wavelength (λ)[9,10]. The coefficient k is the amplitude term representing the concentration and the exponent term S is the spectral slope which indicates the nature of CDOM. This equation, in the form $A(\lambda) = A(\lambda_0)*\exp(-s(\lambda - \lambda_0))$ where λ_0 is a reference wavelength, is customarily used by remote sensing satellites for retrieval of CDOM at desired wavelengths from data at select wavelengths, e.g. 412, 440 (or 443) or 480 nm, which are channels that satellite sensors are often equipped with.

The value of S calculated from commonly used and so-called single exponential model (SEM)[11,12] of spectral absorbance (or absorption coefficient) used in CDOM retrieval is 0.014 nm^{-1} for ocean water[13] and 0.016 nm^{-1} for river water[14]. The average slope of different ecosystems has been found to vary widely between ca. 0.010 (ref. 15) and 0.023 nm^{-1} (ref. 16), and the actual values can range between 0.005 and 0.040 nm^{-1}. The chemical factors influencing S are molecular weight, aromaticity and presence of specific light absorbing compounds such as quinones[1,8,17]. In tropical monsoonal estuaries in which river water flow can vary from nil during summer to flood scale during monsoon season, the *in situ* and terrestrial fluxes of CDOM can oscillate between extremes, and hence the abiogenic, e.g. sorptive and photochemical processes and biogenic, e.g. bacterial and metabolic processes magnify the complexity of the CDOM absorption spectra[1,8].

CDOM values calculated from slope values can vary widely. The increase in slope from 0.01 to 0.023 nm^{-1} will lower the CDOM estimate to less than a third at 550 nm using 440 nm as the reference wavelength. In the frequently reported S range ca. 0.012–0.018 nm^{-1}, CDOM is underestimated by 75%. This implies that the usual practice of adopting the average S for an ecosystem even as it is widely variable within the ecosystem in algorithms of remote sensors is fraught with built-in errors. Precise determination of S is an essential requirement for accurate estimate of CDOM. Ideally, it would be desirable to eliminate S in CDOM calculations.

Deviations from the ideal exponential curve of CDOM occur mainly due to peaks in specific regions of the absorption spectrum, e.g. the 260–280 nm peak, due to protein and/or humic structural moieties in the source DOM, and during DOM alteration. If in the CDOM absorption curve, a sufficiently broad region occurs which is (relatively) least affected by these processes, the S of this spectral region would approximate the CDOM exponential character better than any other region. And if this S is related to CDOM outside the region, then that S-CDOM model relationship can be used to predict CDOM at desired wavelengths.

Our objectives were to (i) identify a spectral region that in most samples (spectra) is free from absorption peaks/shoulders and compute S for this region, (ii) identify a wavelength or group of wavelengths at which the CDOM is best related to S, and (iii) derive CDOM at other wavelengths for possible application in satellite remote sensing. The study is based on long-term sampling in contrasting estuaries for a wider application.

Over 800 water samples were collected during six years from a large tropical (Godavari) estuary and a year in an organic-rich coastal (Chilika) lagoon which behaves like an estuary.

Among the global rivers, the Godavari ranks 34th and 32nd in catchment area (310×10^3 sq. km) and water discharge (105 km^3) respectively[18,19]. It is a monsoonal river, and 75% of its discharge takes place during the 4-month period from July to October (monsoon period). During other months (non-monsoon period), the influx is allowed to accumulate in the reservoir so that the stored water is available for release into the irrigation canals of the intensively cultivated deltaic plain. Its estuarine complex covers an area of 330 sq. km. The Gautami–Godavari that flows towards the east is larger than the south flowing Vasishtha Godavari estuary. The Gautami–Godavari estuary was sampled at four stations (Supplementary Figure 1 *a*) during 2010–2016. Station 1 is the upper estuary (UE) (water depth, 10 m), and stations 2–4 constitute the lower estuary (LE) (15, 5, 5 m respectively). Thirty four field campaigns (Supplementary Figure 1 *b*) were conducted during which water samples were collected at surface, 5, 10 and 15 m depths, yielding 11 samples per campaign, i.e. 374 samples in all.

The Chilika is a shallow (depth, 1–3 metres) brackish water lagoon with estuarine character connected to the Bay of Bengal through a narrow mouth, and fed by a large number of monsoonal rivers (Supplementary Figure 1 *c*)[20]. It is the second largest lagoon globally and its water spread extends over 1150 sq. km during peak monsoon when the rivers are in flood. During summer, the area reduces to 900 sq. km and the salinity increases in the outer channel (Supplementary Figure 1 *c*) to oceanic or even higher values due to the prevalent evaporative condition. Due to its unique ecosystem, it is a protected wetland under the Ramsar Convention, 1981. For some time the lagoon was included in the threatened 'Montreux' record but was later (in the year 2002) removed from this list due to the conservational efforts of the Government. Water samples were collected at surface for one year during 12 monthly campaigns at 36 stations (432 samples in all).

Seawater samples were collected using 5 litre Niskin bottle on mechanized vessels. A Seabird CTD was used for onboard measurements. Water samples (100 ml each) were drawn for CDOM measurement from the Niskin

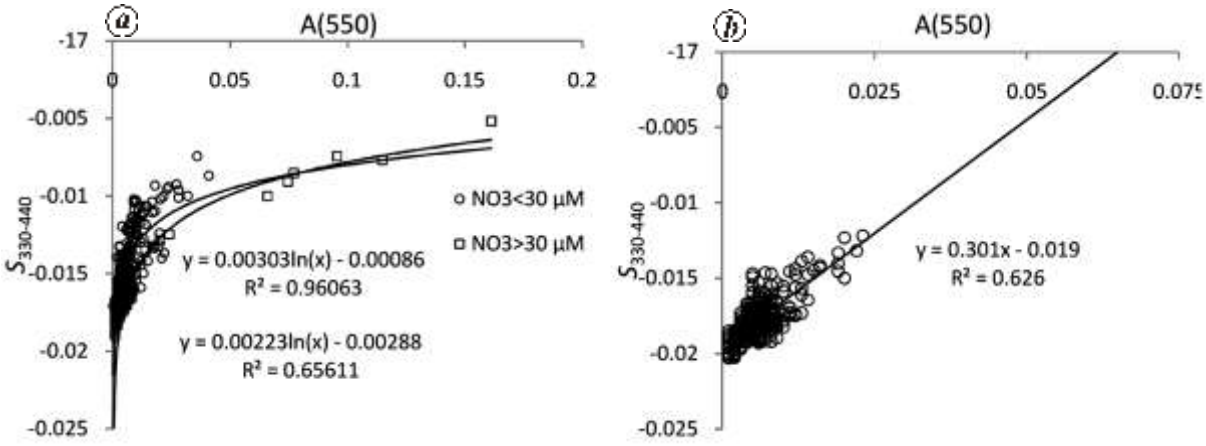

Figure 1. Scatter plots of $A(\lambda)$ and $S_{330-440}$ at 550 nm: ***a***, Godavari estuary (samples with nitrate <30 and >30 µM are shown as circles and squares respectively); ***b***, Chilika lagoon (highest nitrate encountered was 30 µM).

bottle into pre-cleaned (with chromic acid) and pre-combusted (450°C, 3 h) amber coloured glass bottles with teflon cap followed by preservation in an ice box (4°C). The ice box was transported to the laboratory within 3–6 hours of collection. In the laboratory, the samples were first equilibrated to room temperature (22° ± 1°C) and filtered in dim light through 0.22 µm millipore polycarbonate membrane filters. The filters were soaked in milliQ water for 5 min just before filtration. Allowing an uniform equilibration time of 15 minutes, the absorbance of filtered samples was measured. Typically, the CDOM spectral measurements were completed within 6–12 h of sample collection.

Absorbance spectra of the nearly 800 samples were obtained between 200 and 800 nm at 1 nm intervals on Shimadzu UV-Visible 1800 spectrophotometer using 10 cm path length quartz cells and using milliQ (organic free) water as reference. In all samples, the optical density at 700 nm, A(700) was low (0.0000 ± 0.0010); however for the sake of uniformity, spectral correction was made by nulling A(700)[21]. Spectral slope, S was calculated by nonlinear exponential curve fit of absorbance on wavelength[12] for different spectral regions including the regions of 330–440, 300–500 and 275–295 nm. Further details of precautions and the accuracy of measurement of CDOM are given in our other studies[22–24].

Detailed examination by magnifying spectral regions of CDOM absorption spectra revealed peaks or shoulders in some spectra at 200–220 nm, sharp, 255–295 nm, broad, and in a few samples 360–390 nm, broad (Supplementary Figure 2). By repeated exponential curve fitting of different spectral ranges, a spectral region was identified in which >95% of samples produced an exponential fit of the CDOM absorbance (A) on λ with the coefficient of determination (R^2) approaching unity. This was the 330–440 nm region. At $\lambda < 330$ nm, the peaks/shoulders at ~270 nm and ~220 nm distorted the slope and thereby decreased its statistical significance. At $\lambda > 440$ nm, the absorbance in quite a few samples was so low that the measurement accuracy decreased, which also decreased the significance of the slope.

The spectral slope ($S_{330-440}$) was calculated using the SEM procedure in an excel sheet. The $S_{330-440}$ ranged between –0.0052 and –0.0215 (average ± standard deviation = 0.0152 ± 0.0027 nm^{-1}) in the estuary and between –0.0066 and –0.0223 nm^{-1} (–0.0179 ± –0.0017) in the lagoon. It was related to CDOM absorbance in the visible region ca 550 nm (Figure 1). The strength of the $A(\lambda)$–$S_{330-440}$ (linear) relationship, measured as R^2 was high in the visible ranges of 540–600 nm in the Godavari estuary and 550–650 nm in the lagoon (Figure 2).

Repeating correlation analysis on the data of other spectral ranges did not produce results of comparable statistical confidence levels as with the 330–440 nm range. The cases of the wider 300–500 nm range ($S_{300-500}$) and narrower 275–295 nm ($S_{275-295}$) were considered for comparison with $S_{330-440}$. In the estuary and the lagoon, the $S_{275-295}$ was highly scattered against $S_{330-440}$ (figure not shown). The $S_{300-500}$ did follow a linear trend against $S_{330-440}$ producing significant fits of $S_{330-440} = 0.8445 \times S_{300-500} - 0.0024$ ($R^2 = 0.95$, $n = 370$) for the estuary, and $S_{330-440} = 0.8445 \times S_{300-500} - 0.0029$ ($R^2 = 0.94$, $n = 430$) for the lagoon (Supplementary Figure 3 *a*, *b*). The two slopes are identical at 0.0155 nm^{-1} in the estuary and at 0.0188 nm^{-1} in the lagoon (Supplementary Figure 3 *c*). However, significant deviations occurred at other spectral slopes, which undermined the spectral slope – $A(\lambda)$ relationships.

By using $S_{330-440}$, the model spectra were calculated. Two methods of computing the model spectra were adopted: (i) The coefficient model: The $A(\lambda)$ was initially plotted on λ in the 330–440 nm region, and the (exponential) regression parameters thereof noted. The exponent term which represents the spectral slope ($S_{330-440}$) was in turn related to the coefficient (k) of the regression procedure through another highly significant ($P < 0.0001$) relationship (Supplementary Figure 4). As k can now be

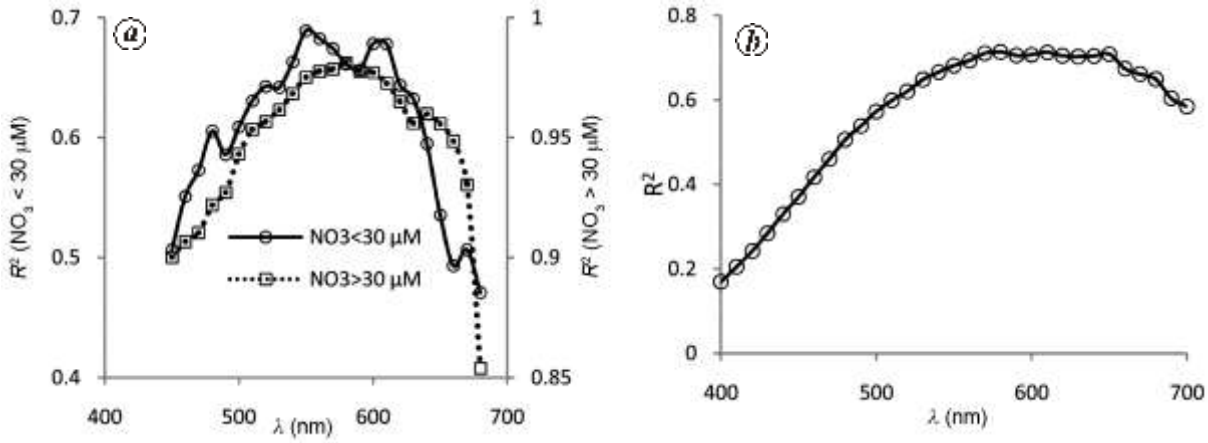

Figure 2. Scatter plots of R^2 of the $A(\lambda)$-$S_{330–440}$ relationship and wavelength (λ) as an indicator of the strength of the relationship: ***a***, Godavari estuary; ***b***, Chilika lagoon. The λ at which best significance occurs is around 550 nm.

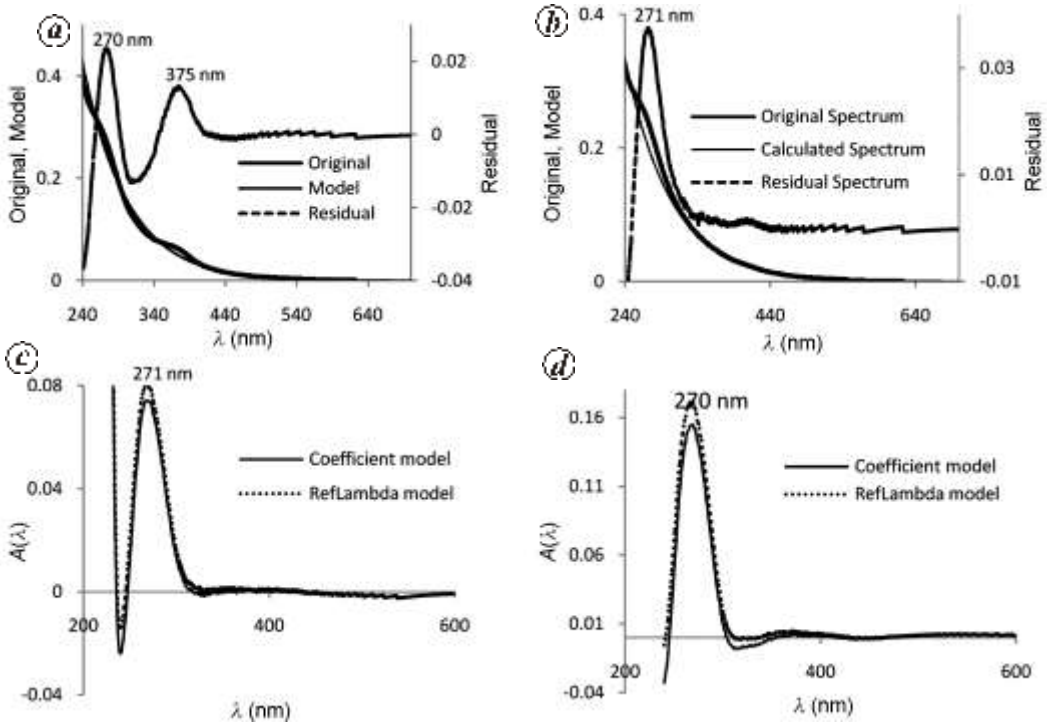

Figure 3. Residual (actual–model) spectra. The model spectra were calculated from $S_{330–440}$ by (***a***) using the equation $A(\lambda) = k.\exp(-s\lambda)$ (coefficient model) for Godavari estuary on 19 May 2011 and also by, (***b***) using $A(\lambda) = A(\lambda_0) \times \exp(-s(\lambda - \lambda_0))$ (RefLambda model) where the reference wavelength (λ_0) was 440 nm on 6 January 2011, (***c***) as in (***a***) and (***b***) during monsoon (September 2011, St. 8) and (***d***) non-monsoon (May 2012, St. 10) in the Chilika lagoon.

expressed in terms of S in the equation $A(\lambda) = k \cdot e^{-s\lambda}$, the model spectrum can be calculated. (ii) Reflambda model: In the equation $A(\lambda) = A(\lambda_0) \times \exp(-s(\lambda - \lambda_0))$, $A(440)$ was used as the reference, and the model spectrum calculated. The choice of 440 nm was because of its extensive use in remote sensing studies.

The residual spectra were calculated by subtracting the model spectra from the observed spectra, and they contained peaks which were not apparent in the original spectra (Figure 3). In particular, a prominent peak appeared at ~270 nm.

Phytoplankton, plants, bacteria, higher organisms, soil, aerosol, etc. contribute CDOM to various degrees in the hydrosphere[1,5]. Further, CDOM is in a state of continuous construction to larger, more condensed structures as well as degradation by enzymatic, bacterial and photochemical

processes to smaller molecules. Accordingly, the CDOM absorption (and fluorescence) properties and shapes of the UV-visible spectra of natural waters (CDOM), and the spectral slopes vary significantly[1,5]. In the UV region, besides CDOM, inorganic species, e.g. nitrate, nitrite, Fe(II) and Cr(VI) also have absorptions. In particular, the intense peak at 200–220 nm is attributed to nitrate, and its intensity (A(220)) used for the estimation of nitrate[25]. The peaks at ~270 nm and 365 nm are attributed to CDOM in natural waters[1,5], in phytoplankton cultures[26] and during macroalgae degradation[27].

Spectral slope has been calculated for different wavelength ranges as reviewed in Helms *et al.*[28] and Loiselle *et al.*[29], the underlying assumption being that the spectrum is exactly exponential over the spectral range(s) considered[11]. A broader range, e.g. 300–700 nm region reveals the average structure of CDOM[1] while narrower ranges such as 275–295 nm, 350–400 nm (ref. 28) and the 20 nm band over the entire absorption spectrum producing what is known as the 'spectral slope curve'[29], help gain insight into specific structural moieties in the CDOM polymeric structure. The CDOM is (inversely) related to S (refs 1, 5) but the relationship has not been constrained for broader application. The $S_{330–440}$ appears better suited to capture both the CDOM parameters of its structure and concentration. The 110 nm range for the slope calculation is between the broader range of 200 nm in the case of $S_{300–500}$ (and 400 nm in the case of $S_{300–700}$) and the narrower range of 20 nm in the case of $S_{275–295}$ (and 50 nm in the case of $S_{350–400}$).

It has been suggested[11] that the deviations from the SEM could be accounted for with better statistical significance by considering alternative models of CDOM spectra. However, these models introduce non-descript, sample-specific elements such as variable exponential behaviour and regression constants that are difficult to parameterize. Modelling via $S_{330–440}$ offers a simpler alternative without compromising on the exponential character of CDOM spectra. In most spectra (~95% of samples), the ~365 nm peak (shoulder) is either non-existent or weak and did not cause the exponential character of the 330–440 nm region to significantly deviate. The influence of the ~270 nm peak ceased at and beyond 330 nm, and at $\lambda > 440$ nm, the CDOM absorbance was too low in some samples either due to low levels of source CDOM or due to preferential photo-induced loss or blue shifted CDOM products[11,30].

Massiotte and Markager[31] performed Gaussian modelling of the CDOM absorption spectra after removing the peaks, by an iterative procedure until the fall of absorbance with wavelength obeyed the exponential law. The residual spectra consisting of these peaks are then the unaccounted deviations of the modelling procedure (figure 2 *c*, *d* in Massicotte and Markager[31]). The residual spectra shown in Figure 3 are similar to and agree with the residual spectra based on Gaussian modelling of Massicotte and Markager[31]. The $S_{330–440}$ is a simpler alternative to construct the model spectra and identify the spectral absorptions of the coloured components that accompany or are part of the chemically complex CDOM. Since $S_{330–440}$ can be constrained in terms of A(550) as shown (Figure 1), the model spectra were then computed from the equation: $A(\lambda) = A(550) \times \exp(550 - \lambda)\{p \ln A(550) + q\}$ where p is the coefficient term and q is the constant term in the logarithmic equation between $A(550)$ and $S_{330–440}$.

Several factors restrict the constraining of CDOM and its spectral slope. They include (i) lack of statistical confidence in the CDOM-spectral slope relationship, (ii) for no consensus several spectral ranges that have been used in studies for the calculation of S and (iii) the lack of statistical confidence of the single exponential model fit of CDOM on wavelength. The $S_{330–440}$ proposed in this study appears to overcome these issues and constrain CDOM better. The effect of inorganic components such as nitrate is minimal in this region. CDOM at ~550 nm can be used as reference to derive CDOM at desired λ from the exponential equation. The model constants are unique for each estuary. Further study is being done to test the applicability of the model elements to more estuaries, and within an estuary, to investigate spatio-temporal factors.

1. Coble, P. G., Marine optical biogeochemistry: the chemistry of ocean color. *Chem. Rev.*, 2007, **107**, 402–418.
2. Fichot, C. G. and Benner, R., A novel method to estimate DOC concentrations from CDOM absorption coefficients in coastal waters. *Geophys. Res. Letts.*, 2011, **38**(3), doi:10.1029/2010GL046152.
3. Rochelle-Newall, E. J. and Fisher, T. R., Chromophoric dissolved organic matter and dissolved organic carbon in Chesapeake Bay. *Mar. Chem.*, 2002, **77**(1), 23–41; doi:10.1016/S0304-4203(01)00073-1.
4. Asmala, E., Autio, R., Kaartokallio, H., Pitkanen, L., Stedmon, C. A. and Thomas, D. N., Bioavailability of riverine dissolved organic matter in three Baltic Sea estuaries and the effect of catchment land use. *Biogeoscience*, 2013, **10**, 6969–6986.
5. Nelson, N. B. and Siegel, D. A., The global distribution and dynamics of chromophoric dissolved organic matter. *Ann. Rev. Mar. Sci.*, 2013, **5**, 447–476.
6. Harvey, E. T., Kratzer, S. and Andersson, A., Relationships between coloured dissolved organic matter and dissolved organic carbon in different coastal gradients of the Baltic Sea. *Ambio*, **44**(3), 2015, S392–S401; doi:10.1007/s13280-015-0658-4.
7. Gonçalves-Araujo, R., Stedmon, C. A. and Heim, B., Dubinenkov, I., Kraberg, A., Moiseev, D. and Bracher, A., From fresh to marine waters: characterization and fate of dissolved organic matter in the Lena River delta region, Siberia. *Front. Mar. Sci.*, 2015, **2**, 108; doi: 10.3389/fmars.2015.00108.
8. Siegel, D. A., Maritorena, S., Nelson, N. B., Behrenfeld, M. J. and McClain, C. R., Colored dissolved organic matter and its influence on the satellite-based characterization of the ocean biosphere. *Geophys. Res. Lett.*, 2005, **32**(20), L20605–L20608; doi:10.1029/2005GL024310.
9. Jerlov, N. G., *Optical Oceanography*, Elsevier, New York, 1976, p. 194.
10. Shifrin, K. S., Physical Optics of Ocean Water American Institute of Physics, College Park, MD, 1988, p. 285.

11. Twardowski, M. S., Boss, E., Sullivan, J. M. and Donaghay, P. L., Modelling the spectral shape of absorption by chromophoric dissolved organic matter. *Mar. Chem.*, 2004, **89**, 69–88.
12. Stedmon, C. A. and Markager, S., Behavior of the optical properties of coloured dissolved organic matter under conservative mixing. *Estuar. Coastal Shelf Sci.*, 2003, **57**, 973–979.
13. Bricaud, A., Morel, A. and Prieur, L., Absorption by dissolved organic matter of the sea (yellow substance) in the UV and visible domains. *Limnol. Oceanogr*., 1981, **26**(1), 43–53.
14. Bowers, D. G. and Brett, H. L., The relationship between CDOM and salinity in estuaries: An analytical and graphical solution. *J. Mar. Syst.*, 2008, **73**(1–2), 1–7; http://doi.org/10.1016/j.jmarsys.2007.07.001.
15. Clark, C. D., Litz, L. P. and Grant, S. B., Salt marshes as a source of chromophoric dissolved organic matter (CDOM) to Southern California coastal waters. *Limnol. Oceanogr.*, 2008, **53**(5), 1923–1933.
16. Højerslev, N. K. and Aas, E., Spectral light absorption by yellow substance in the Kattegat–Skagerrak area. *Oceanologia*, 2001, **43**, 39–60.
17. Cory, R. M. and McKnight, D. M., Fluorescence spectroscopy reveals ubiquitous presence of oxidized and reduced quinones in dissolved organic matter. *Environ. Sci. Technol.*, 2005, **39**(21), 8142–8149.
18. Rao, K. L., India's Water Wealth, Its Assessment, Uses and Projections, Orient Longman, New Delhi, 1975.
19. Gaillardet, J., Dupre, B., Louvat, P. and Allegre, C. J., Global silicate weathering and CO_2 consumption rates deduced from the chemistry of large rivers. *Chem. Geol*., 1999, **159**, 3–30.
20. Sarkar, S., Bhattacharya, A., Bhattacharya, A., Satpathy, K., Mohanty, A. and Panigrahi, S., Chilika lake. In *Encyclopedia of lakes and reservoirs* (eds Bengtsson, L., Herschy, R. W. and Fairbridge, R. W.), Springer, 2012, vol. 953, pp. 148–155.
21. Shank, C. G., Nelson, K. and Montagna, K., Importance of CDOM distribution and photo reactivity in a shallow Texas Estuary. *Estuar. Coast*, 2009, **32**, 661–677.
22. Chari, N. V. H. K., Sarma, N. S., Pandi, S. R. and Murthy, K. N., Seasonal and spatial constraints of fluorophores in the midwestern Bay of Bengal by PARAFAC analysis of excitation emission matrix spectra. *Estuar. Coastal Shelf Sci*., 2012, **100**, 162–171.
23. Pandi, S. R. *et al.*, Contrasting phytoplankton community structure and associated light absorption characteristics of the western Bay of Bengal. *Ocean Dynam.*, 2014, doi:10.1007/s10236-013-0678-1.
24. Chiranjeevulu, G. *et al.*, Colored dissolved organic matter signature and phytoplankton response in a coastal ecosystem during mesoscale cyclonic (cold core) eddy. *Mar. Environ. Res.*, 2014, **98**, 49–59; doi:10.1016/j.marenvres.2014.03.002.
25. Edwards, A. C., Hooda, P. S. and Cook, Y., Determination of nitrate in water containing dissolved organic carbon by ultraviolet spectroscopy. *Int. J. Environ. Anal. Chem.*, 2001, **80**(1), 49–59; doi:10.1080/03067310108044385.
26. Chari, N. V. H. K., Keerthi, S., Sarma, N. S., Pandi, S. R., Chiranjeevulu, G., Kiran, R. and Koduru, U., Fluorescence and absorption characteristics of dissolved organic matter excreted by phytoplankton species of western Bay of Bengal under axenic laboratory condition. *J. Exp. Mar. Biol. Ecol.*, 2013, **445**, 148–155.
27. Hulatt, C. J., Thomas, D. N., Bowers, D. G., Norman, L. and Zhang, C., Exudation and decomposition of chromophoric dissolved organic matter (CDOM) from some temperate macroalgae. *Estuar. Coastal Shelf Sci.*, 2009, **84**, 147–153.
28. Helms, J., Stubbins, A., Ritchie, J. D., Minor, E., Kieber, D. J. and Mopper, K., Absorption spectral slopes and slope ratios as indicators of molecular weight, source, and photobleaching of chromophoric dissolved organic matter. *Limnol. Oceanogr*., 2008, **53**(3), 955–969.
29. Loiselle, S. A., Bracchini, L., Dattilo, A. M., Ricci, M., Tognazzi, A., Cézar, A. and Rossi, C., The optical characterization of chromophoric dissolved organic matter using wavelength distribution of absorption spectral slopes. *Limnol. Oceanogr.*, 2009, **54**(2), 590–597; doi:10.4319/lo.2009.54.2.0590.
30. Del Vecchio, R. and Blough, N., Spatial and seasonal distribution of chromophoric dissolved organic matter and dissolved organic carbon in the Middle Atlantic Bight, *Mar. Chem.*, 2004, **89**, 169–187.
31. Massicotte, P. and Markager S., Using a Gaussian decomposition approach to model absorption spectra of chromophoric dissolved organic matter, *Mar. Chem.*, 2016, **180**, 24–32.

ACKNOWLEDGEMENTS. We acknowledge financial assistance from INCOIS (Indian National Coastal and Oceanographic Information Services) through grant nos. INCOIS/093/2007 and INCOIS:F&A: XII:D2:023 and Integrated Coastal and Marine Area Management (ICMAM) through Grant no. MoES/ICMAM-OD/11th Plan/2005. We declare no conflict of interest.

Received 28 February 2017; accepted 8 November 2017

doi: 10.18520/cs/v114/i08/1762-1767

Impact of elevated CO_2 on *Oryza sativa* phenology and brown planthopper, *Nilaparvata lugens* (Hemiptera: Delphacidae) population

G. Guru-Pirasanna-Pandi[1,3,]*, Subhash Chander[1], Madan Pal[2] and P. S. Soumia[1]

[1]Division of Entomology,
[2]Division of Plant Physiology, Indian Agricultural Research Institute, New Delhi 110 012, India
[3]Division of Crop Protection, National Rice Research Institute, Cuttack 753 006, India

The impact of elevated CO_2 (570 ± 25 ppm) on brown planthopper, *Nilaparvata lugens* (Stål) and Pusa Basmati 1401 rice in comparison to ambient CO_2 was studied in open top chambers (OTCs) during the rainy seasons of 2013 and 2014. Crop canopy circumference was higher (13.1–16.8 cm) under elevated CO_2 when compared to ambient CO_2 (10.3–13.1 cm) during different rice phenological stages indicating the positive influence of elevated CO_2. In addition, elevated CO_2 exhibited a positive effect on rice plants through increase in tiller number (17.6%), reproductive tiller

*For correspondence. (e-mail: guruagri@gmail.com)